ZAMM · Z. Angew. Math. Mech. **95**, No. 5, 433 – 443 (2015) / **DOI** 10.1002/zamm.201300183

The effect of noise on the response of a vertical cantilever beam energy harvester

Michael I. Friswell[1,*], **Onur Bilgen**[2], **S. Faruque Ali**[3], **Grzegorz Litak**[4], **and Sondipon Adhikari**[1]

[1] College of Engineering, Swansea University, Swansea SA2 8PP, UK
[2] Department of Mechanical and Aerospace Engineering, Old Dominion University, Norfolk, VA 23529, USA
[3] Department of Applied Mechanics, Indian Institute of Technology-Madras, Chennai 600 036, India
[4] Department of Applied Mechanics, Technical University of Lublin, 20-618 Lublin, Poland

Received 7 August 2013, revised 12 February and 11 April 2014, accepted 2 May 2014
Published online 19 May 2014

Key words Energy harvesting, base excitation, random noise, piezoelectric, low frequency, broadband, bifurcation.

An energy harvesting concept has been proposed comprising a piezoelectric patch on a vertical cantilever beam with a tip mass. The cantilever beam is excited in the transverse direction at its base. This device is highly nonlinear with two potential wells for large tip masses, when the beam is buckled. For the pre-buckled case considered here, the stiffness is low and hence the displacement response is large, leading to multiple solutions to harmonic excitation that are exploited in the harvesting device. To maximise the energy harvested in systems with multiple solutions the higher amplitude response should be preferred. This paper investigates the amplitude of random noise excitation where the harvester is unable to sustain the high amplitude solution, and at some point will jump to the low amplitude solution. The investigation is performed on a validated model of the harvester and the effect is demonstrated experimentally.

1 Introduction

The energy limitations of portable power sources is a fundamental bottleneck in many applications. Ambient energy from a variety of sources, such as solar, wind, thermal gradients or mechanical vibration can be harvested and used to provide the energy required. There is significant research and development in the use of smart materials for energy harvesting in applications ranging from battery-free pace-makers (Karami and Inman [26]) to structural health monitoring of civil or aerospace structures (Beeby et al. [4], Priya [38], Lefeuvre et al. [27, 28]). Reviews of the literature on energy harvesting from vibration have been given by Sodano et al. [49], Anton and Sodano [2], Cook-Chennault et al. [9] and Priya and Inman [39]. Furthermore, Pellegrini et al. [37] and Harne and Wang [24] have recently presented focused reviews on the topic of nonlinear vibration energy harvesting.

Piezoelectric materials are widely used as actuators and sensors for active vibration control of beams and plates. Cantilever type vibration energy harvesting devices, such as beams, use a passive substrate to support a piezoelectric transduction element. The maximum power output of such a device, operating in the linear regime, occurs when the fundamental frequency of the device is near the dominant frequency of ambient vibration, ensuring a resonance response that maximizes the strain in the piezoelectric material. Sodano et al. [48, 50] investigated the transduction performance of several monolithic and piezocomposite devices. Electromechanical models and experimental validation were presented by Erturk and Inman [15], and Erturk et al. [13]. Bilgen [5] compared resistive shunt energy harvesting of several cantilever beam vibration energy harvesters. Guyomar et al. [23] and Wickenheiser et al. [53] gave further examples of analysis and maximization of mechanical and electronic parameters of vibration energy harvesters. Ng and Liao [35], duToit et al. [12], Roundy [43], and Renno et al. [42] proposed methods to optimize the parameters of such systems to maximize the harvested energy. Shu and Lien [46, 47], and Shu et al. [45] conducted detailed analyses of power output response of piezoelectric energy harvesting systems. Karami and Inman [25] presented the electromechanical modeling of a low frequency zigzag micro energy harvester.

One of the drawbacks of linear energy harvesters, regardless of the type of its active material, is that generally they are efficient only when the excitation frequency is near to the resonance frequency (see Daqaq [11]). Therefore, most linear energy harvesting devices are designed on the assumption that the (base) excitation has some known narrow-band form, typically harmonic excitation. However, there are many situations where energy harvesting devices are operating under

* Corresponding author E-mail: m.i.friswell@swansea.ac.uk, Phone: +44 1792 602969, Fax: +44 1792 295676

unknown or random excitations, and in such situations harvesters with a broadband or adaptive response are likely to be beneficial. One approach is to adaptively change the parameters of the linear harvester so that its natural frequency becomes close to the excitation frequency as it changes (see Wang et al. [52]). Such adaptive systems may be difficult to implement in general and also may not adapt well to a broadband excitation. Ferrari et al. [19] used an array of cantilever beam harvesters tuned to different frequencies.

An alternative approach to maximize the harvested energy over a wide range of excitation frequencies uses nonlinear structural systems, and a range of devices have been proposed by Cottone et al. [10] and Gammaitoni et al. [21, 22]. The key aspect of the nonlinear harvesters is the use of a double well potential function, so that the device will have two equilibrium positions (see Cottone et al. [10], Mann and Owens [30], Ramlan et al. [41], Ferrari et al. [18], and Quinn et al. [40]). Gammaitoni et al. [21] and Masana and Daqaq [32] highlighted the advantages of a double well potential for energy harvesting, particularly when inter-well dynamics are excited. The simplest equation of motion with a double well potential is the well-known Duffing oscillator, which has been extensively studied, particularly for sinusoidal excitation. The dynamics is often complex, sometimes with coexisting periodic solutions, and sometimes exhibiting a chaotic response. The Duffing oscillator model has been used for many energy harvesting simulations, with the addition of electromechanical coupling for the harvesting circuit. One popular implementation of such a potential is a piezomagnetoelastic system based on the magnetoelastic structure that was first investigated by Moon and Holmes [34] as a mechanical structure that exhibits strange attractor motions. Erturk et al. [14] investigated the potential of this device for energy harvesting when the excitation is harmonic and demonstrated an order of magnitude larger power output over the linear system (without magnets) for non-resonant excitation. One problem with multiple solutions to harmonic excitation is that the system can respond in the low amplitude solution; Sebald et al. [44] proposed a method to excite the system to jump to the high amplitude solution at low energy cost. Stanton et al. [51] and Erturk and Inman [16] investigated the dynamic response of such systems, including the chaotic response. Cottone et al. [10] used an inverted beam with magnets and also considered random excitation. Mann and Sims [31] and Barton et al. [3] used an electromagnetic harvester with a cubic force nonlinearity. Litak et al. [29] and Ali et al. [1] investigated nonlinear piezomagnetoelastic energy harvesting under random broadband excitation. McInnes et al. [33] investigated the stochastic resonance phenomena for a nonlinear system with a double potential well.

Another requirement of an energy harvester is to be able to harvest reasonable amount of energy when the excitation frequency is low. Common examples include the vibration of long span bridges and tall buildings. A low frequency piezoelastic or piezomagnetoelastic harvester is difficult to realise due to the small physical dimensions of the devices. In this paper an inverted cantilever beam with a piezoelectric patch loaded with a tip mass is investigated. The idea is to adjust the mass such that the system is near buckling and therefore has a low effective resonance frequency. The beam undergoes large deformations exhibiting nonlinear behavior and hence geometric nonlinearities are considered. By exploiting this nonlinearity, the aim is to have a low frequency energy harvesting device which is relatively insensitive to a particular excitation frequency and responds with a relatively large amplitude. Friswell et al. [20] presented an experimentally validated concept of an inverted cantilever beam with tip mass subjected to harmonic excitations. Borowiec et al. [8] analyzed the efficiency of the inverted cantilever beam, focusing on the region of stochastic resonance where the beam motion has a large amplitude. Numerical analysis showed that increasing the noise level allows the motion of the beam system to escape from single well oscillations and thus generate more power.

This paper considers the electromechanical response of the pre-buckled inverted cantilevered beam subjected to a combination of harmonic and broadband random excitation. This extends the work of Friswell et al. [20] which concentrated on pure sinusoidal excitation. In reality, systems driven by sinusoidal base excitation, for example from machinery rotating at a fixed spin speed, will also be subject to broadband excitation from ambient sources. Therefore the effect of this random noise on the deterministic steady state response to sinusoidal excitation must be investigated and understood. In particular, for nonlinear systems with multiple solutions, the high amplitude solution is preferred for energy harvesting; the addition of random noise can cause the system to jump to the low amplitude solution, which is a situation that should be avoided. White noise base displacement is selected as the random signal, where the signal has a uniform power spectral density. An experimental system is also built to validate the model and to demonstrate the effects identified by the simulations.

2 The inverted beam with tip mass

The nonlinear energy harvesting system consists of an inverted elastic beam with a tip mass and the base is harmonically excited in the transverse direction. Friswell et al. [20] derived the governing equation of motion using Euler-Bernoulli beam theory. The displacement-curvature relation of the beam is nonlinear due to the large transverse displacement of the beam. Figure 1 shows the beam as a vertical cantilever of length L with harmonic base excitation $z(t) = z_0 \cos \omega t$. The beam carries a concentrated tip mass, M_t, with moment of inertia I_t; in this paper this mass is assumed to be located at the end

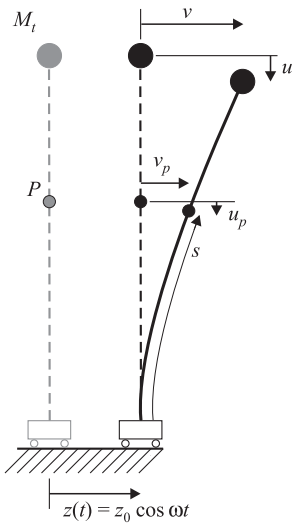

Fig. 1 Schematic of the inverted beam harvester. M_t denotes the tip mass attached to the elastic beam, while v and u denote the horizontal and vertical displacements of the mass. In this paper piezoelectric patches are placed along the beam but are not shown here.

of the beam. The horizontal and vertical elastic displacements at the tip mass are v and u, respectively, and s represents the distance along the neutral axis of the beam.

The horizontal displacement at any point in the beam is represented as a function of the tip mass displacement through a function for the beam deformation, $\psi(s)$, as

$$v_p(s,t) = v_p(L,t)\psi(s) = v(t)\psi(s) \tag{1}$$

where $v(t) = v_p(L,t)$ is the horizontal displacement of the tip mass. A suitable displacement model is [17]

$$\psi(s) = \left(1 - \cos\left(\frac{\pi s}{2L}\right)\right). \tag{2}$$

Using this displacement model the equation of motion in terms of the horizontal displacement v and electrical voltage V is

$$\begin{aligned}&\left[N_5^2 I_t + M_t + \rho A N_1 + \left(\rho A N_3 + M_t N_4^2 + N_5^4 I_t\right) v^2\right] \ddot{v} + \left[\rho A N_3 + M_t N_4^2 + N_5^4 I_t\right] v \dot{v}^2 \\ &\quad + \left[EIN_6 - N_9 \rho A g - N_4 M_t g + 2EIN_7 v^2\right] v - \Theta_1 V - \Theta_2 v^2 V = -\left[\rho A N_2 + M_t\right] \ddot{z}\end{aligned} \tag{3}$$

where the constants N_1 to N_9 are

$$\begin{aligned}
N_1 &= \left(\frac{3\pi - 8}{2\pi}\right) L, & N_2 &= \left(\frac{\pi - 2}{\pi}\right) L, & N_3 &= \left(\frac{\pi^2(2\pi^2 - 9)}{384}\right) \frac{1}{L}, \\
N_4 &= \left(\frac{\pi^2}{8}\right) \frac{1}{L}, & N_5 &= \left(\frac{\pi}{2}\right) \frac{1}{L}, & N_6 &= \left(\frac{\pi^4}{32}\right) \frac{1}{L^3}, \\
N_7 &= \left(\frac{\pi^6}{2^9}\right) \frac{1}{L^5}, & N_8 &= \left(\frac{\pi^8}{4096}\right) \frac{1}{L^7}, & N_9 &= \left(-\frac{1}{4} + \frac{1}{16}\pi^2\right).
\end{aligned} \tag{4}$$

In the following sections, the base acceleration, $\ddot{z}(t)$, will consist of an harmonic component (already described) and a random component. The random component is a band limited white noise displacement signal but will be characterised by the standard deviation of the corresponding acceleration signal.

The model of the piezoelectric patches are now considered. The mechanical stiffness and mass density of the piezoelectric layers may be included in the beam constants already derived, although in this paper an alternative approach is taken, where the stiffness parameters, N_6 and N_7, are updated based on the experimental data. The electromechanical coupling constants are

$$\Theta_1 = \gamma_c \psi'(L_c) \qquad \text{and} \qquad \Theta_2 = \frac{1}{2}\gamma_c (\psi'(L_c))^3 \tag{5}$$

Table 1 Parameter values used in the simulation.

Beam and tip mass			Energy harvester		
ρ	7850	kg/m^3	L_c	28	mm
E	210	GN/m^2	γ_c	-1.49×10^{-5}	Nm/V
b	15.88	mm	C_p	25.7	nF
h	0.245	mm	R_l	9.944	MΩ
L	287	mm	Θ_1	-1.245×10^{-5}	C/m
M_t	10.5	g	Θ_2	-4.345×10^{-6}	C/m^3
I_t	0				

where L_c is the active length of the piezoelectric material, which is assumed to start at the clamped end of the beam. For a unimorph configuration with excitation in the 31 mode, with thickness h_c and width b_c, the constant γ_c is

$$\gamma_c = E_c d_{31} b_c \left(h + \frac{h_c}{2} - \bar{z} \right) \tag{6}$$

where h is the thickness of the beam, d_{31} is the piezoelectric constant, E_c is the Young's modulus of the piezoelectric material, and $\bar{z}$ is the effective neutral axis [36]. These expressions assume a monolithic piezoceramic actuator perfectly bonded to the beam; Bilgen et al. [7] considered the effect of the structure of a Macro-Fiber Composite (MFC) on the coupling coefficient, and also the effect of the bond and the insulating Kapton layers.

On the electrical side the piezoelectric patches may be considered as a capacitor, and the electrical circuit is represented by a resistive shunt connected across the piezoelectric patch. The electrical equation then becomes

$$C_p \dot{V} + \frac{V}{R_l} + \Theta_1 \dot{v} + \Theta_2 v^2 \dot{v} = 0 \tag{7}$$

where R_l is the load resistor and C_p is the capacitance of the piezoelectric patch.

The average power scavenged between times T_1 and T_2 is calculated as

$$P_{ave} = \frac{1}{T_2 - T_1} \int_{T_1}^{T_2} \frac{V(t)^2}{R_l} \mathrm{d}t. \tag{8}$$

3 Numerical simulations

The parameters considered for the numerical simulations are given in Table 1, which were verified by the experiments reported by Friswell et al. [20]. Note that the increase in beam stiffness due to the Macro-Fiber Composite (MFC) required an increase in the N_6 and N_7 terms of 19% and 0.57%, respectively. The beam-mass system is excited at the base with harmonic excitation with amplitude $z_0 = 15$ mm.

To demonstrate that multiple solutions occur for the deterministic inverted beam system with the given parameters, Fig. 2 shows the RMS steady state values of the displacement as the frequency of excitation is swept up and then down. This figure is obtained by numerically integrating the equations of motion at each excitation frequency and allowing the transients to decay leaving a stable steady state solution. The final state vector for the current excitation frequency is then used as the initial conditions for the next excitation frequency, thus simulating a frequency sweep. For the range of frequencies considered, there are two stable periodic solutions, distinguished by the amplitude of the response as the low and high amplitude solutions. Two excitation frequencies, namely $\omega = 0.501$ Hz and $\omega = 0.515$ Hz, will be chosen to demonstrate the effect of noise on the steady state response.

Consider now the case when $\omega = 0.515$ Hz, which is in middle of the frequency region of multiple solutions. Figure 3 shows the basin of attraction of the low and high amplitude solutions, where the high amplitude solution is given in black. Time simulations are now used to test the effect of random forcing on the steady state arising from the sinusoidal excitation at a frequency of $\omega = 0.515$ Hz. First, the initial conditions are set to obtain the high amplitude solution by using the basin of attraction in Fig. 3, and for the first 20 s of the simulation the random forcing is set to zero to enable the steady state response to develop. Then the amplitude of the random forcing component is linearly increased over 20 s. It should be emphasised that the basin of attraction is only defined for the deterministic case; with the inclusion of random excitation, then any particular set of initial conditions would yield a probability that each potential solution would occur (providing the solutions may be suitably categorised). The random forcing is white noise base displacement with a bandwidth of 5 Hz (due to the limitations

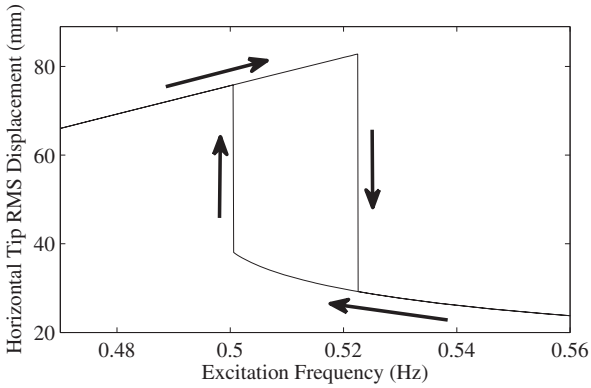

Fig. 2 The RMS displacement response of the tip mass as the excitation frequency varies. The arrows show the directions of the frequency sweeps.

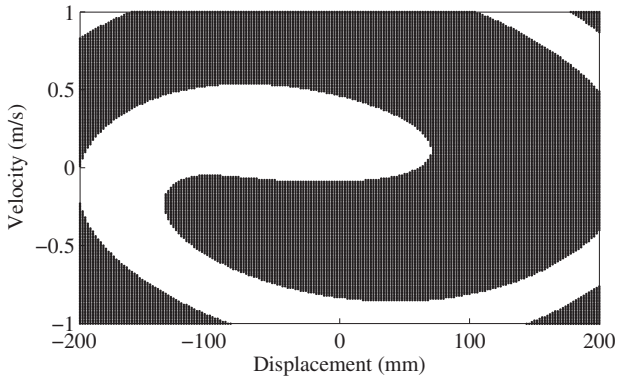

Fig. 3 Basin of attraction of the high amplitude solution for $\omega = 0.515$ Hz for the deterministic system. Black represents the high amplitude solution.

of the experimental system). The tip displacement response, and the corresponding average electrical power output, is then computed to determine if the system is responding in the high or low amplitude solution. Figure 4(b) shows the resulting average power as the noise level is increased. For low noise levels (below a standard deviation of $3000\,\text{mm/s}^2$) the high amplitude response is maintained, but for high levels of random forcing (above a standard deviation of $4000\,\text{mm/s}^2$) the low amplitude response is preferred. For intermediate noise levels the response starts at the high amplitude solution and at some time instant will jump to the low amplitude solution; this indicates that the low amplitude and low energy solution is preferred at this excitation frequency, although there is also a small probability that the response will jump back to the high amplitude solution. In Fig. 4 the low and high amplitude solution trends are clear; if the response jumps between solutions then the resulting average power is between the power output from the high and low amplitude solutions. Figure 4(b) shows that, at high noise levels, the response can jump to the high amplitude solution. If initial conditions are chosen so that the low amplitude solution is obtained, before adding the random forcing, the results in Fig. 4(a) are obtained. In this case, the high amplitude solution is never obtained until the noise level is very high (above a standard deviation of $5000\,\text{mm/s}^2$).

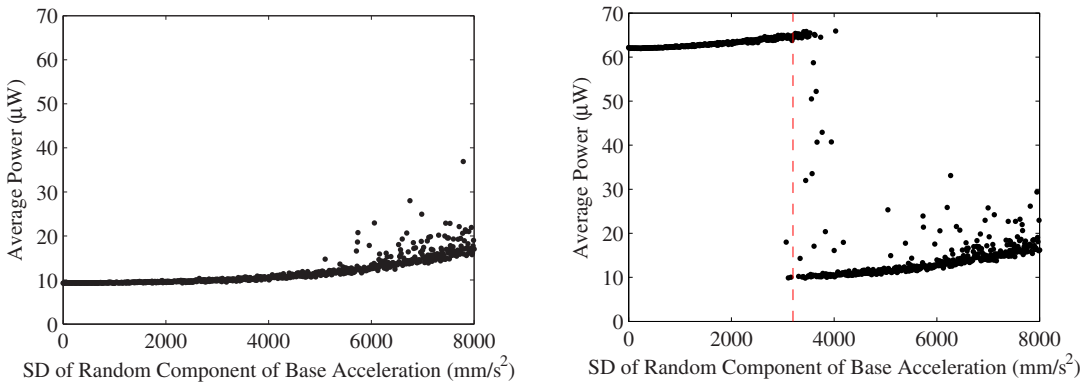

(a) Low amplitude solution (b) High amplitude solution

Fig. 4 The effect of the random component of the excitation on the low and high amplitude steady state solutions. The harmonic excitation has $\omega = 0.515$ Hz and $z_0 = 15$ mm. The amplitude of the random component is given by the standard deviation (SD).

Suppose that the initial conditions are chosen to give the high amplitude steady state solution, as shown in Fig. 4(b). We now chose white noise displacement with a standard deviation of 7.25 mm (equivalent to an acceleration with a standard deviation of $3200\,\text{mm/s}^2$) and perform a Monte-Carlo simulation with 1000 samples to obtain the probability density function (pdf) of the time when the response first jumps from the high amplitude solution to the low amplitude solution. Figure 5 shows the pdf obtained using the kernel density estimator in MATLAB. The decaying pdf looks similar to a Poisson distribution, which would occur if the probability of a jump at a particular time was independent of the time since

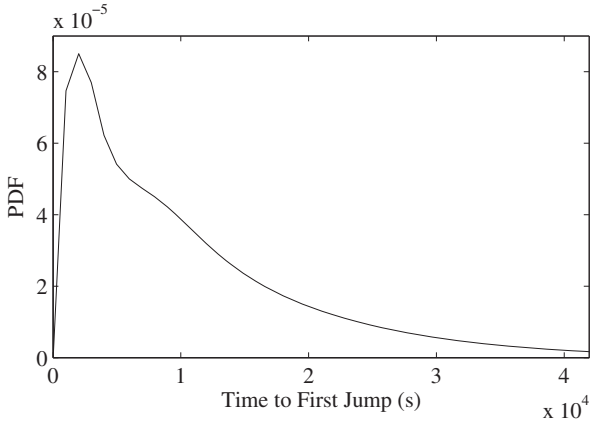

Fig. 5 The probability density function (pdf) for the time when the response first jumps from the high to the low amplitude solution. The harmonic component of the excitation has $\omega = 0.515$ Hz and $z_0 = 15$ mm and the noise component of the acceleration has a standard deviation of 3200 mm/s^2 (corresponding to the vertical dashed line in Fig. 4(b)).

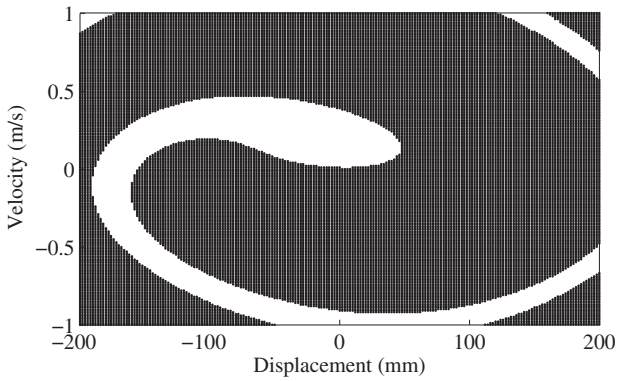

Fig. 6 Basin of attraction of the high amplitude solution for $\omega = 0.501$ Hz for the deterministic system. Black represents the high amplitude solution.

the last jump. Of course, for practical energy harvesting, the objective would be to sustain the high amplitude solution, and hence the random component of the base acceleration should have a standard deviation lower than 3000 mm/s^2.

Suppose now these simulations are repeated at an excitation frequency of $\omega = 0.501$ Hz, which is close to the lowest excitation frequency where multiple solutions occur (see Fig. 2). Figure 6 shows the basin of attraction of the high amplitude solution (in black) and shows that the high amplitude region is much larger than the case when $\omega = 0.515$ Hz, shown in Fig. 3. Figure 7(a) shows the result of increasing the noise level when starting from the low amplitude solution. At this excitation frequency, the basin of attraction of the low amplitude solution is much smaller and hence the beam is more likely to jump to the high amplitude solution. Similarly, when starting from the high amplitude solution, the level of noise has to be larger at this excitation frequency before jumps to the low amplitude solution occur.

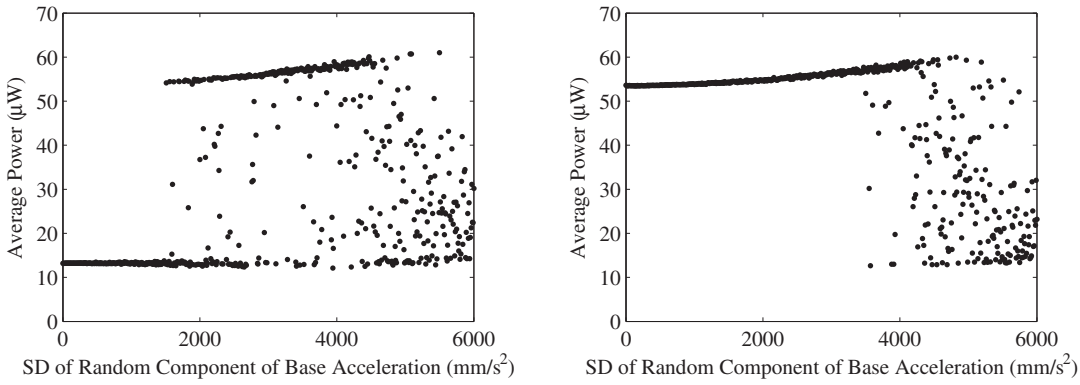

(a) Low amplitude solution (b) High amplitude solution

Fig. 7 The effect of the random component of the excitation on the low and high amplitude steady state solutions. The harmonic excitation has $\omega = 0.501$ Hz and $z_0 = 15$ mm. The amplitude of the random component is given by the standard deviation (SD).

4 Experimental testing

An experimental system was built to demonstrate the effects simulated in the previous section. A direct validation of the model is difficult because of unmodeled nonlinearities (e.g. piezoelectric hysteresis, out-of-plane motion, etc) and because the single degree of freedom model for the beam is insufficient at large displacements. However the low amplitude

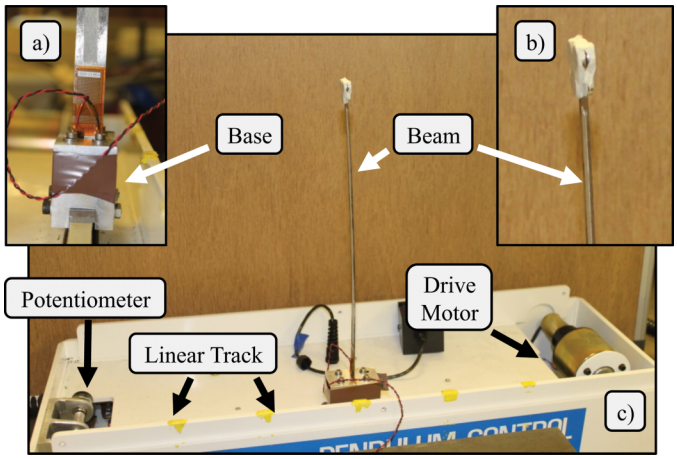

Fig. 8 The experimental setup a) Base of the beam showing the base clamp and the MFC device near the root b) Tip mass of 10.5 g shown nearly vertical at a stable equilibrium c) Linear actuation system with the inverted cantilever beam mounted.

response is used to validate the underlying linear model and estimate material damping, and these parameters are used in the simulations. Furthermore the effects of random noise on the steady state solutions, as shown in the simulations, may be demonstrated and the responses compared qualitatively. Bilgen et al. [6] gives further details of the experiments and gives a more complete set of results.

The experimental system is shown in Fig. 8 and is derived from a Bytronic Pendulum Control System. This device is composed of a belt driven linear slider that moves in a track. The belt is actuated by a control signal applied to the DC motor. A multi-turn potentiometer monitors the position of the belt, hence the position of the linear slider. A displacement feedback controller ensures that the displacement is proportional to the control signal. The linear slider has low inertia and there is no return spring (as in an electromagnetic shaker), and this means that the base motion is affected by small imperfections in the linear track. In addition, since the system is driven by the forcing of the DC motor only (i.e. no return spring), the actual excitation deviates from the desired harmonic excitation near $\dot{z} = 0$ condition. Both of these imperfections in the excitation waveform are measured by the potentiometer; however their effects on the general motion and the power output of the harvester are initially assumed negligible. The input dynamics of the linear actuator can be represented by the displacement-to-voltage-input frequency response which is shown in Fig. 9. The measurement of input-dynamics confirms that the static response of the linear actuator is as expected. Attenuation occurs as the desired output displacement magnitude is increased. For the current tests, where the random noise bandwidth is 5 Hz, the attenuation will be small.

A clamping mechanism, which applies uniform pressure across the clamped surface of the beam, is attached to the linear slider. Note that all experiments presented in this paper are conducted without removing the beam from the clamp; therefore consistent boundary conditions are achieved across all cases. A beam made of spring steel of thickness 0.245 mm, width 15.88 mm and free length 293 mm is used as the inverted cantilever. The tip mass is implemented using several disk-like neodymium magnets with a diameter of 10 mm, a height of 5 mm and an approximate weight of 1.75 g each, whose positions could be moved easily. In the model the tip mass is assumed to be at the end of the beam; the portion of the beam above the magnets in the experiment is assumed to have negligible effect on the dynamic behavior of the system but could be included in the model if desired. For this demonstration a single tip mass of 10.5 g (i.e. six magnets), was used, giving an effective beam length of 287 mm. This tip mass is just below the buckling threshold of the beam.

A single piezocomposite patch, the Macro-Fiber Composite (MFC) model M2814-P2 manufactured by Smart Material Corp., of active length 28 mm and active width 14 mm is bonded to the beam near the clamped end in a unimorph configuration. The patch is aligned to the beam symmetrically in the widthwise direction and as close to the base as possible. The MFC is adhered to the beam using a 3M DP460 type two-part epoxy and cured under a vacuum.

The response of the beam is characterised by its transverse displacement and power output through a resistive shunt. A load resistor is used to characterise the energy harvesting performance instead of other passive or active circuits; therefore the analysis is focused on the fundamental nonlinear dynamic behaviour of the cantilever energy harvester. The signals of interest are measured using a National Instruments (NI) 9215 analog-to-digital (A/D) module with 16 bit resolution (set to ± 10 V range) at a fixed sampling rate of 100 Hz. Two signals are measured: the potentiometer output which is proportional to the base displacement; and the voltage output of the MFC piezocomposite device. The control signal was produced by an NI 9263 cDAQ module with 16 bit resolution (set to ± 10 V range) at a generation rate of 10 kHz. This control signal was low-pass (LP) filtered using a Kemo (Type VBF/24) elliptic filter with a 5 Hz cut-off frequency to minimise the high frequency noise from the digital-to-analog converter (DAC).

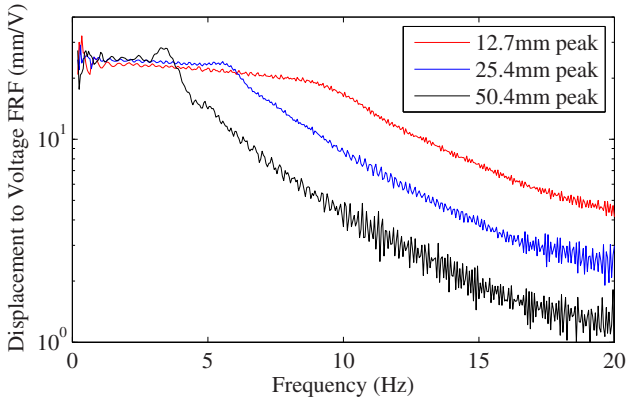

Fig. 9 Displacement to voltage frequency response of the feedback-controlled linear actuator. The three lines correspond to different peak displacement amplitudes of the actuator.

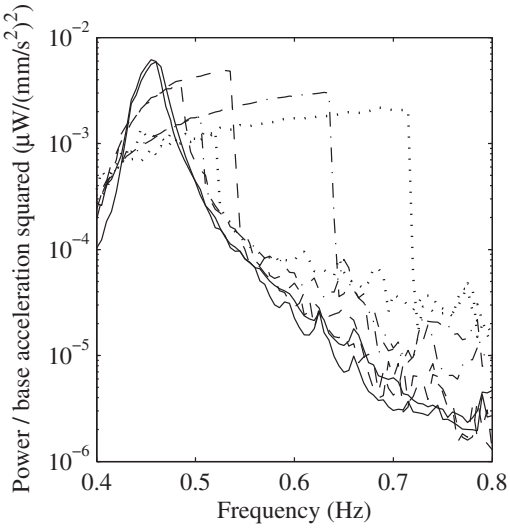

Fig. 10 The measured average harvested power for a tip mass of $M_t = 10.5$ g, and a base excitation with amplitudes of $z_0 = 5$ (solid), 10 (dashed), 15 (dash-dot) and 20 mm (dotted) at a range of frequencies. $R_l = 9.944\,\mathrm{M\Omega}$ for $z_0 = 5$ and 10 mm, and $R_l = 3.344\,\mathrm{M\Omega}$ for $z_0 = 15$ and 20 mm.

The deterministic response to harmonic excitation is demonstrated first. The frequency of excitation was swept in both increasing and decreasing directions, and this process was repeated for a range of base excitation amplitudes. The beam was excited for 30 complete cycles (of base excitation) but only the last 10 cycles were recorded and analysed, to minimise the effect of transient motion. Since the frequency was incremented in small steps and the waveform was continuous between each frequency, the disturbance (e.g. rapid accelerations) to the beam was minimised. This is important since such disturbances may trigger a premature transition to the alternative solution as the frequency is increased and decreased. Figure 10 shows the resulting response for a number of base excitation amplitudes. Note the characteristic amplitude jumps caused by the frequency induced bifurcations.

We now demonstrate the effect of noise on the steady state response and the probability of jumping from one solution to the other. Figure 11 shows the average power generated as a function of the amplitude of the random noise excitation quantified by the average of the absolute base acceleration. The coding of the markers and the line types is used to identify

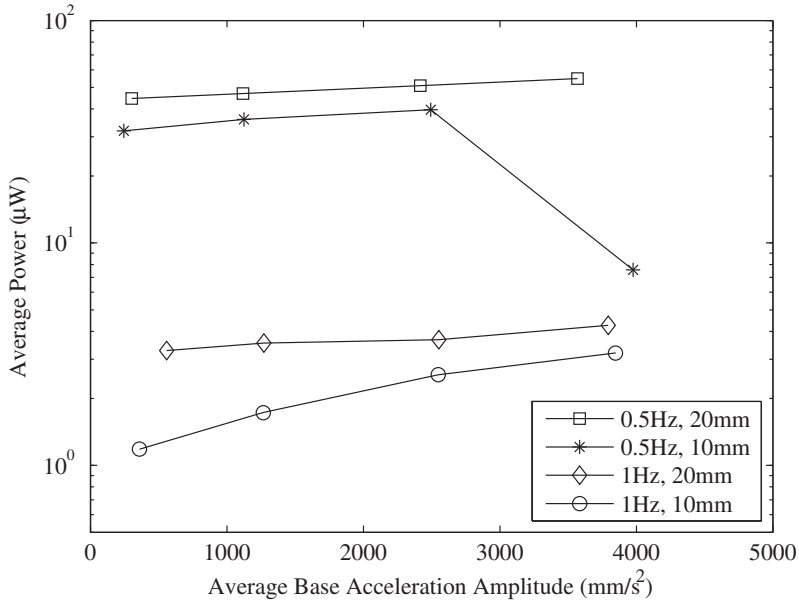

Fig. 11 The measured average harvested power for a combined random and harmonic base excitation, as a function of increasing amplitude of random acceleration, for the final 24% of the acquisition period. The lines represent the frequency and amplitude of the harmonic excitation, as given in the legend. The load resistance was $R_L = 5.05\,\mathrm{M\Omega}$ and the random excitation filter cut-off was 5 Hz.

different characteristics of the experimental system, and most of the features in the figure are readily explained. Clearly the power harvested increases significantly when the harmonic excitation is close to the resonance (i.e. excitation at 0.5 Hz). The average power also increases with noise amplitude, and this increase is more marked when the sinusoidal excitation is away from resonance. As expected, more power is generated when the amplitude of the harmonic excitation is larger. The load resistance is fixed at $5.05\,\mathrm{M}\Omega$, although because the electromechanical coupling is low, the effect of the load resistance is negligible in most cases. There is one data point in Fig. 11 that does not follow the expected trends, namely the base excitation at about $4000\,\mathrm{mm/s^2}$ for the harmonic base excitation at 0.5 Hz with 10 mm amplitude. This is the case with the noise amplitude at just the right level to cause jumping between the multiple steady state solutions.This agrees qualitatively with the simulated results which highlighted that jumping between solutions occurred at higher noise levels, although in the experiments it is difficult to control which solution the system initially exhibits. Furthermore, the simulations will contain modelling errors, for example the deformation shape of the beam does not correspond perfectly to the single mode approximation, and the nonlinear response is very sensitive to system parameters and the excitation frequency.

The harmonic excitation signal is now fixed at 10 mm amplitude and 0.5 Hz frequency, and a $9.994\,\mathrm{M}\Omega$ load resistor is used. White noise displacement with a range of amplitudes and band limited to 5 Hz is added to the harmonic signal. Figure 12 shows the measured voltage as the base excitation noise level increases. For low noise levels, i.e. a standard deviation of 7.1 mm and below, the beam responds in the high amplitude solution. When the standard deviation increases to 10.4 mm the beam initially responds in the low amplitude solution but jumps to the high amplitude solution at about 150 s. This result confirms the non-resonant solution destabilisation at a certain level of noise amplitude, and this case corresponds qualitatively to Fig. 7(a), where the basin of attraction of the low amplitude solution (with the smallest area, see Fig. 6) is disturbed by noise. The power generated is directly related to the amplitude of response and hence these results are consistent with the observations on Fig. 11.

5 Conclusion

The proposed energy harvesting system addresses a very difficult problem where energy is required from a structure with low excitation frequency and high displacement, such as a highway bridge. A resonant linear harvester based on a cantilever beam is difficult to implement because the low natural frequency requires a very large or a very flexible beam. In this paper, a low frequency piezoelectric energy harvester is investigated using an inverted elastic beam-mass system subjected to a

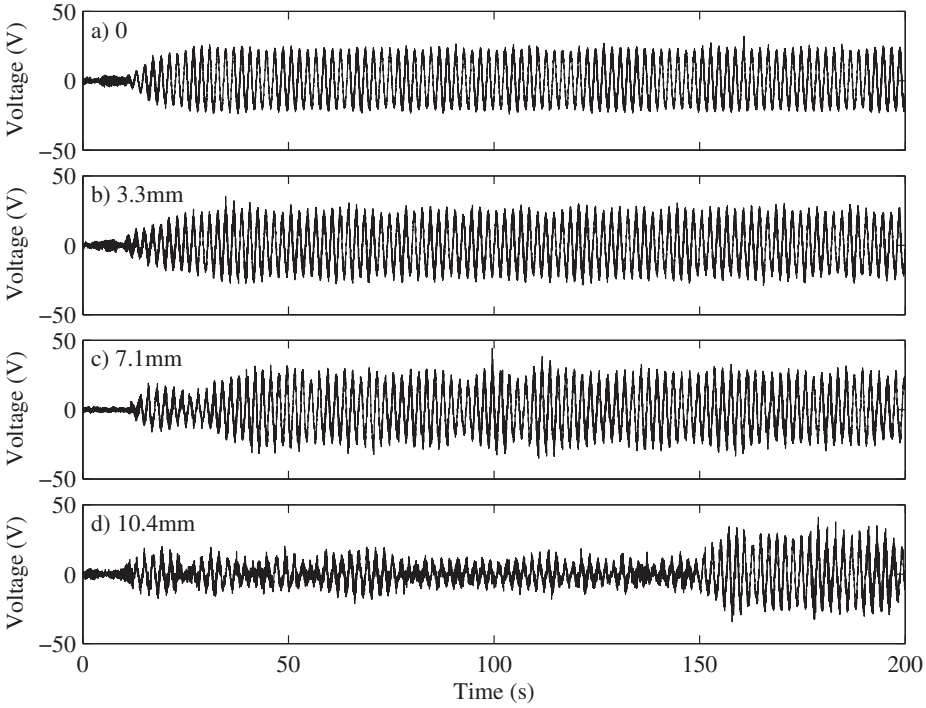

Fig. 12 The voltage response of the inverted cantilever beam with harmonic excitation of amplitude 10 mm and frequency 0.5 Hz, and additive white noise base displacement with increasing standard deviation (SD): a) no noise b) SD 3.3 mm c) SD 7.1 mm d) SD 10.4 mm.

combined sinusoidal and random base excitation. For certain ranges of frequency of sinusoidal excitation the device has two periodic solutions, and the high amplitude response is preferred as the energy harvested will be greater. The addition of random noise causes the response to jump between the low to high amplitude solutions, and the probability of each solution occurring depends on the parameters of the system. To ensure the maximum harvested energy either an active control system should be used to cause the device to jump to the high amplitude solution, or the device should be designed so that the high amplitude solution is preferred. Further work is required to investigate the relationship between the basins of attraction of the deterministic system and the probability of the high amplitude solution occurring, and the impact on the design and operation of the harvester.

Acknowledgements The authors acknowledge the funding of the EPSRC through the Engineering Nonlinearity programme grant, EP/K003836. Dr. Ali acknowledges funding from the Royal Society through a Newton Fellowship. Prof. Litak acknowledges the support of the Polish National Science Center under grant agreement 2012/05/B/ST8/00080. Prof. Adhikari gratefully acknowledges the support of Royal Society through a Wolfson Research Merit Award.

References

[1] S. F. Ali, S. Adhikari, M. I. Friswell, and S. Narayanan, The analysis of magnetopiezoelastic energy harvesters under broadband random excitations, J. Appl. Phys. **109**, 074904 (2011).
[2] S. R. Anton and H. A. Sodano, A review of power harvesting using piezoelectric materials (2003–2006), Smart Mater. Struct. **16**(3), R1–R21 (2007).
[3] D. A. W. Barton, S. G. Burrow, and L. R. Clare, Energy harvesting from vibrations with a nonlinear oscillator, Journal of Vibration and Acoustics **132**(021009) (2010).
[4] S. P. Beeby, M. J. Tudor, and N. M. White, Energy harvesting vibration sources for microsystems applications, Meas. Sci. Technol. **17**(12), R175–R195 (2006).
[5] O. Bilgen, Aerodynamic and Electromechanical Design, Modeling and Implementation of Piezocomposite Airfoils, PhD thesis, Mechanical Engineering (Virginia Tech, Blacksburg, VA, USA, 2010).
[6] O. Bilgen, S. F. Ali, M. I. Friswell, G. Litak, and M. de Angelis, Non-Linear Piezoelectric Vibration Energy Harvesting from a Vertical Cantilever Beam with Tip Mass, in: Conference on Smart Materials, Adaptive Structures and Intelligent Systems (SMASIS2013, Utah, 2013).
[7] O. Bilgen, A. Erturk, and D. J. Inman, Analytical and experimental characterization of macro-fiber composite actuated thin clamped-free unimorph benders, J. Vib. Acoust. **132**(5), 051005 (2010).
[8] M. Borowiec, G. Litak, M. I. Friswell, S. F. Ali, S. Adhikari, A. W. Lees, and O. Bilgen, Energy harvesting in piezoelastic systems driven by random excitations, Int. J. Struct. Stab. Dyn. **13**(7), 1340006 (2013).
[9] K. Cook-Chennault, N. Thambi, and A. Sastry, Topical review: Powering mems portable devices – a review of non-regenerative and regenerative power supply systems with special emphasis on piezoelectric energy harvesting systems, Smart Mater. Struct. **17**, 043001 (2008).
[10] F. Cottone, H. Vocca, and L. Gammaitoni, Nonlinear energy harvesting, Phys. Rev. Lett. **102**, 080601 (2009).
[11] M. Daqaq, Response of a uni-modal Duffing-type harvesters to random force excitations, J. Sound Vib. **329**, 3621–3631 (2010).
[12] N. duToit, B. Wardle, and S. Kim, Design considerations for mems-scale piezoelectric mechanical vibration energy harvesters, Integr. Ferroelectr. **71**, 121–160 (2005).
[13] A. Erturk, S. R. Anton, O. Bilgen, and D. J. Inman, Effect of Material Constants and Mechanical Damping on Piezoelectric Power Generation, in: 22nd Biennial Conference on Mechanical Vibration and Noise (ASME, New York, 2009), pp. 513–522.
[14] A. Erturk, J. Hoffmann, and D. J. Inman, A piezomagnetoelastic structure for broadband vibration energy harvesting, Appl. Phys. Lett. **94**, 254102 (2009).
[15] A. Erturk and D. J. Inman, A distributed parameter electromechanical model for cantilevered piezoelectric energy harvesters, J. Vib. Acoust. Trans. ASME **130**, 041002 (2008).
[16] A. Erturk and D. J. Inman, Broadband piezoelectric power generation on high-enery orbits of the bistable Duffing oscillator with electromechanical coupling, J. Sound Vib. **330**, 2339–2353 (2011).
[17] E. Esmailzadeh and G. Nakhaie-Jazar, Periodic behavior of a cantilever beam with end mass subjected to harmonic base excitation, Int. J. Non-Linear Mech. **33**(4), 567–577 (1998).
[18] M. Ferrari, V. Ferrari, M. Guizzetti, B. Ando, S. Baglio, and C. Trigona, Improved energy harvesting from wideband vibrations by nonlinear piezoelectric converters, Sens. Actuators A, Phys. **162**, 425–431 (2010).
[19] M. Ferrari, V. Ferrari, M. Guizzetti, D. Marioli, and A. Taroni, Piezoelectric multifrequency energy converter for power harvesting in autonomous microsystems, Sens. Actuators A, Phys. **142**, 329–335 (2008).
[20] M. Friswell, S. Ali, O. Bilgen, S. Adhikari, A. Lees, and G. Litak, Nonlinear piezoelectric vibration energy harvesting from a vertical cantilever beam with tip mass, J. Intell. Mater. Syst. Struct. **23**(11), 1505–1521 (2012).
[21] L. Gammaitoni, I. Neri, and H. Vocca, Nonlinear oscillators for vibration energy harvesting, Appl. Phys. Lett. **94**, 164102 (2009).
[22] L. Gammaitoni, I. Neri, and H. Vocca, The benefits of noise and nonlinearity: extracting energy from random vibrations, Chem. Phys. **375**, 435–438 (2010).
[23] D. Guyomar, G. Sebald, S. Pruvost, M. Lallart, A. Khodayari, and C. Richard, Energy harvesting from ambient vibrations and heat, J. Intell. Mater. Syst. Struct. **20**(5), 609–624 (2008).

[24] R. L. Harne and K. W. Wang, A review of the recent research on vibration energy harvesting via bistable systems, Smart Mater. Struct. **22**, 023001 (2013).
[25] M. A. Karami and D. J. Inman, Electromechanical modeling of the low-frequency zigzag micro-energy harvester, J. Intell. Mater. Syst. Struct. **22**(3), 271–282 (2011).
[26] M. A. Karami and D. J. Inman, Powering pacemakers from heartbeat vibrations using linear and nonlinear energy harvesters, Appl. Phys. Lett. **100**, 042901 (2012).
[27] E. Lefeuvre, A. Badel, A. Benayad, L. Lebrun, C. Richard, and D. Guyomar, A comparison between several approaches of piezoelectric energy harvesting, J. Phys. IV (France) **128**, 177–186 (2005).
[28] E. Lefeuvre, A. Badel, C. Richard, L. Petit, and D. Guyomar, A comparison between several vibration-powered piezoelectric generators for standalone systems, Sensors and Actuators A: Physical **126**(2), 405–416 (2006).
[29] G. Litak, M. I. Friswell, and S. Adhikari, Magnetopiezoelastic energy harvesting driven by random excitations, Appl. Phys. Lett. **96**(21), 214103 (2010).
[30] B. P. Mann and B. A. Owens, Investigations of a nonlinear energy harvester with a bistable potential well, J. Sound Vib. **329**, 1215–1226 (2010).
[31] B. P. Mann and N. D. Sims, Energy harvesting from the nonlinear oscillations of magnetic levitation, J. Sound Vib. **319**(1–2), 515–530 (2009).
[32] R. Masana and M. F. Daqaq, Relative performance of a vibratory energy harvester in mono- and bi-stable potentials, J. Sound Vib. **330**, 6036–6052 (2011).
[33] C. McInnes, D. Gorman, and M. Cartmell, Enhanced vibrational energy harvesting using nonlinear stochastic resonance, J. Sound Vib. **318**(4–5), 655–662 (2010).
[34] F. Moon and P. Holmes, A magnetoelastic strange attractor, J. Sound Vib. **65**(2), 275–296 (1979).
[35] T. Ng and W. Liao, Sensitivity analysis and energy harvesting for a self-powered piezoelectric sensor, J. Intell. Mater. Syst. Struct. **16**(10), 785–797 (2005).
[36] C. Park, C. Walz, and I. Chopra, Bending and torsion models of beams with induced-strain actuators, Smart Mater. Struct. **5**, 98–113 (1996).
[37] S. P. Pellegrini, N. Tolou, M. Schenk, and J. L. Herder, Bistable vibration energy harvesters: A review, J. Intell. Mater. Syst. Struct. **24**(11), 1303–1312 (2013).
[38] S. Priya, Advances in energy harvesting using low profile piezoelectric transducers, J. Electroceram. **19**(1), 165–182 (2007).
[39] S. Priya and D. Inman, Energy Harvesting Technologies (Springer, Berlin, Heidelberg, New York, 2008).
[40] D. D. Quinn, A. L. Triplett, L. A. Bergman, and A. F. Vakakis, Comparing linear and essentially nonlinear vibration-based energy harvesting, J. Vib. Acoust. **133**, 011001 (2011).
[41] R. Ramlan, M. J. Brennan, B. R. Mace, and I. Kovacic, Potential benefits of a non-linear stiffness in an energy harvesting device, Nonlinear Dyn. **59**, 545–558 (2010).
[42] J. M. Renno, M. F. Daqaq, and D. J. Inman, On the optimal energy harvesting from a vibration source, J. Sound Vib. **320**(1-2), 386–405 (2009).
[43] S. Roundy, On the effectiveness of vibration-based energy harvesting, J. Intell. Mater. Syst. Struct. **16**(10), 809–823 (2005).
[44] G. Sebald, H. Kuwano, D. Guyomar, and B. Ducharne, Experimental Duffing oscillator for broadband piezoelectric energy harvesting, Smart Mater. Struct. **20**, 102001 (2011).
[45] Y. C. Shu, I. Lien, and W. Wu, An improved analysis of the sshi interface in piezoelectric energy harvesting, Smart Mater. Struct. **16**(6), 2253–2264 (2007).
[46] Y. Shu and I. Lien, Analysis of power output for piezoelectric energy harvesting systems, Smart Mater. Struct. **15**(6), 1499–1512 (2006).
[47] Y. Shu and I. Lien, Efficiency of energy conversion for a piezoelectric power harvesting system, J. Micromech. Microeng. **16**(11), 2429–2438 (2006).
[48] H. A. Sodano, G. Park, and D. J. Inman, An investigation into the performance of macro-fiber composites for sensing and structural vibration applications, Mech. Syst. Signal Process. **18**, 683–697 (2004).
[49] H. Sodano, D. Inman, and G. Park, A review of power harvesting from vibration using piezoelectric materials, Shock Vib. Digest **36**, 197–205 (2004).
[50] H. A. Sodano, J. Lloyd, and D. J. Inman, An experimental comparison between several active composite actuators for power generation, Smart Mater. Struct. **15**(5), 1211–1216 (2006).
[51] S. C. Stanton, C. C. McGehee, and B. P. Mann, Nonlinear dynamics for broadband energy harvesting: investigation of a bistable piezoelectric inertial generator, Physica D **239**(10), 640–653 (2010).
[52] L. Wang, T. J. Kazmierski, B. M. Al-Hashimi, S. P. Beeby, and D. Zhu, An Automated Design Flow for Vibration-Based Energy Harvester Systems, in: Design, Automation and Test in Europe Conference and Exhibition, 20–24 April 2009 (IEEE, Nice, France, 2009), pp. 1391–1396.
[53] A. M. Wickenheiser and E. Garcia, Power optimization of vibration energy harvesters utilizing passive and active circuits, J. Intell. Mater. Syst. Struct. **21**(13), 1343–1361 (2010).

